DYNAMIC SHOCK STUDIES OF VANADIUM*

CONF-850770--7

L. C. Chhabildas
Thermomechanical and Physical Division

C. R. Hills
Electron Optics and X-Ray Analysis Division

Sandia National Laboratories
Albuquerque, NM 87185

SAND--85-0322C

DE85 017381

Using gas-gun loading techniques and velocity interferometric techniques, time-resolved wave profiles have been obtained in vanadium over the stress range of 2.9 to 9.7 GPa. These experiments are unique for this material, since there are no Hugoniot measurements available for vanadium below 20.0 GPa. As expected, the risetime data indicate steepened shock structures with increasing shock amplitude. However, unlike aluminum, finite risetimes are determined even at 9.7 GPa, indicating a large effective viscosity for the material. The dynamic yield strength measured at the Hugoniot elastic limit is 0.8 GPa and is approximately twice the static yield strength. Material softening is evidenced through measurements of shock velocity and yield strength determinations in the shocked state. The yield strength of the material upon release from the shocked state is estimated to be ~0.43 GPa and is comparable to the static yield strength. Strain-rate dependent processes may be responsible for a higher elastic shear stress sustained before relaxation to an equilibrium value. The primary mode of deformation in shocked vanadium appears to be cross slip, resulting in dislocation tangles. Deformation twins are also observed in shock-recovered specimens with an increasing number with increased shock stress. The thermal diffusivity for vanadium is low, and the shear-strength loss observed in this material is consistent with the strength loss observed for other materials which also have low thermal diffusivities. It is conceivable that the loss of shear strength may be due to long thermal recovery times resulting from inhomogeneous deformation process. Further studies, such as reshock and shorter pulse-duration experiments, would be useful in providing clues to the apparent material softening behavior.

*This work performed by Sandia National Laboratories supported by the U. S. Department of Energy under contract number DEAC04-76-DP00789.

DISCLAIMER

I. INTRODUCTION

The primary objective of this study was to measure the shock front risetimes in vanadium. Since the advent of time-resolved continuous wave profile measurement techniques [1], Chhabildas and Asay [2] have described a technique to determine an effective shock viscosity for materials from risetime measurements of the wave profiles. The technique has been used to determine the variation of effective viscosity with strain rates for various metals [2-4]. Experimental data to date [5] (where risetime measurements are available), indicate that the strain-rate varies as the fourth power of the shock stress. This fourth power dependence of the strain rate on shock stress has been used by Swegle and Grady [5] to compute the shock risetimes for various materials, including oxides [6,7]. As expected, risetime measurements in vanadium reported in this investigation show steepened shock structures with increasing shock amplitude, although a fourth-power dependence is not conclusively established, due to a limited number of experiments. Although the main emphasis of these experiments was to determine the risetime of the shock front, release structure measurements have allowed a characterization of the mechanical properties of vanadium in the shocked state. In particular, material softening, characteristic of high-strength ceramic materials [8,9], is observed. Similar softening effects have been observed in tungsten [10,11]. These results are also summarized in this paper.

In this investigation, gas gun [12] and velocity interferometric techniques [13] have been used to determine continuous shock loading and release profiles, from which the dynamic shock behavior of vanadium has been inferred. Samples were recovered after each experiment, although no attempt was made to recover samples in special recovery fixtures. In the following sections, the experimental technique is described in detail, and the results of this investigation are reported and discussed. Metallographic analysis of the recovered shock specimens is also discussed in this paper.

II. EXPERIMENTAL TECHNIQUE

The experimental arrangement used for impact studies is indicated in Figure 1. Z-cut sapphire single crystals [14], backed by either a void or PMMA discs, were accelerated on a single-stage compressed gas gun to the desired velocity to obtain impact stresses of 2.9 GPa to 9.7 GPa in the vanadium sample. The projectile velocity was

determined to an accuracy of 0.2% by measuring the transit time of the projectile between two precisely spaced charged pins located on the target plate. Impact tilt was determined by measuring the simultaneity of the projectile surface arrival at an array of charged pins installed flush in the target plate. The average tilt for this series of shots was determined to be approximately 0.5 mrad.

As indicated in Figure 1, the vanadium sample has a Z-cut sapphire single crystal bonded to it. Sapphire was used as an interferometer window [14], since its equation of state is well characterized, and also because its shock impedance is close to that of the vanadium sample. The particle velocity history at the sample-window interface was measured using a velocity interferometer, VISAR. Fringe shifts obtained in the interferometer can be related to the velocity of the reflecting interface.

The interference fringes are detected by three RCA C7291D photomultiplier tubes having a frequency response of 600 MHz. The output of these photomultiplier tubes is then displayed on Tektronix 7104 oscilloscopes using type 7A29 preamplifiers with a frequency response of one GHz. In addition to the photomultiplier tubes and the recording scopes, other sources that contribute to the measured risetime are the delay leg of the interferometer, cables, impact misalignment between the target and the impactor. The composite risetime of the system is ~3 ns [2].

III. RESULTS

WAVE SPEEDS

The vanadium samples used in this investigation had an average density of 6.08 $\pm$ 0.01 g/cm^3, and the grain size varied from 30 μm to 150 μm. The major impurity elements are iron (1000 ppm), magnesium (80 ppm), aluminum (40 ppm), and nickel (30 ppm). Using ultrasonic techniques, the average longitudinal and shear wave speeds were determined to be 6.017 km/s and 2.785 km/s, respectively. Based on these measurements, the average bulk velocity and Poisson's ratio (ν_o) are calculated to be 5.085 km/s and 0.364, respectively.

The impact conditions for the series of experiments are summarized in Table I. The particle velocity histories measured at the sample-window interface are shown in Figure 2. By correlating the impact time with the wave arrival time, the average wave speed of the leading edge of the wave profiles shown in Figure 2 was determined to be 6.15 $\pm$ 0.15 km/s. This average wave speed was used in determining the subsequent

shock wave arrival time in each experiment. It should be noted that the wave speed of the leading edge of the wave agrees with the ultrasonically measured longitudinal wave speed to within a few percent, and hence represents an elastic wave speed. Unlike many metals, the elastic wave is ramped, and the transition from the elastic to plastic wave is not well defined. As seen in Figure 2, the structure is reproducible to an interface velocity of 0.045 km/s in the three experiments, and this is therefore taken to be the elastic limit.

Since finite risetimes are measured, the shock wave arrival time is taken at the mid-point of the plastic wave. The shock wave speeds (U_s) determined from these experiments are given in Table I. Using impedance matching techniques the particle velocity (u_p) behind the shock front in the vanadium sample is calculated from the peak particle velocity measured at the sample-window interface. These values are also reported in Table I. The shock-velocity/particle-velocity data obtained in this investigation is shown plotted against the published U_s -- u_p relation for vanadium [15] obtained from high-pressure experiments in Figure 3. As indicated in the figure, the shock velocity for the experiment at 2.9 GPa lies below the expected value; the measured value of 4.87 km/s for the shock velocity is actually lower than the expected shock velocity of 5.08 km/s for the material. This is believed to be primarily related to material softening over this stress range and will be discussed further in a later section.

SHOCK STRESS AND STRAIN

Since finite risetimes associated with the shock front are measured, an incremental form of the jump conditions, given by the equations

$$\sigma = \sum \rho_o c du, \quad \text{and} \quad \epsilon = \sum du/c, \tag{1,2}$$

was used to estimate the peak shock stress, σ, and strain, ϵ. ρ_o represents the initial density of the material, and c is the Lagrangian wave velocity of the wave corresponding to the material particle-velocity increment du. The values for the peak shock stress and strain are given in Table I. These values for shock stress and strain are plotted in Figure 4. (A two-wave analysis of the wave profiles, assuming a centered elastic wave and a steady plastic wave yielded stress and strain values which agreed to within 0.7% of the values given in Table I.) The average value for the Hugoniot elastic limit (σ_{HEL}) from these experiments is determined to be 1.86

$\pm$ .03 GPa at a volume strain of 0.0086 and a particle velocity of 0.051 km/s. The elastic limit is indicated in Figure 4. Using the relation,

$$\sigma_{HEL} = \frac{(1-\nu_o)}{(1-2\nu_o)}Y, \tag{3}$$

a value of 0.8 GPa is obtained for Y, the yield strength in compression.

A smooth fit to the hydrostatic stress-strain data [16] on vanadium to 10 GPa is also shown in Figure 4. It is assumed that the shock hydrostat is similar to the hydrostatic isotherm determined at these pressures. A comparison of the present Hugoniot states with the hydrostatic data indicates a decrease in the stress deviator (τ) upon dynamic yielding. For the purposes of this discussion, τ is the difference between the shock stress, σ, and the hydrostatic pressure, P. This suggests that the material collapses towards the hydrostat. If the material were elastic-perfectly plastic, then the stress deviator would be a constant and the Hugoniot states would lie on the dotted line indicated in the figure. Admittedly, the stress differences are small, but the low estimate for the shock velocity measured for the wave at 2.9 GPa is also consistent with the implied softening effects. This can be seen from the relation

$$\frac{d\tau}{d\epsilon} = \frac{d\sigma}{d\epsilon} - \frac{dP}{d\epsilon}. \tag{4}$$

The differences are between the value of deviator stress at the HEL and the value in the shocked state. $d\sigma/d\epsilon$ and $dP/d\epsilon$ are proportional to the shock velocity squared and the bulk velocity squared, respectively. Thus, for an elastic-perfectly plastic material for which τ would be a constant, $d\tau/d\epsilon$ would be zero and the shock velocity would be equal to the bulk velocity; for a material that has shear softening $d\tau/d\epsilon$ would be negative, and the shock velocity would then be lower than the expected bulk velocity.

RISETIMES AND SHOCK VISCOSITY

The effective viscosity is defined in terms of the plastic strain rate by the relation [2],

$$\Delta\sigma = \eta\dot{\epsilon}, \tag{5}$$

where η is the effective viscosity, $\dot{\epsilon}$ is the plastic strain rate, and $\Delta\sigma$ is the viscous stress or the overstress. For one-dimensional steady-wave propagation in a viscous medium, the overstress $\Delta\sigma$ is defined as the difference between the stress achieved during deformation and the corresponding equilibrium stress, and is estimated as the

maximum difference between the Rayleigh line and the Hugoniot curve; for small strains this overpressure can be approximated by the relation,

$$\Delta\sigma = \frac{1}{2} s \sigma_f \epsilon_f, \tag{6}$$

where σ_f and ϵ_f are the final Hugoniot stress and strain states achieved during shock compression, and s is the slope of the shock velocity (U_s)-particle velocity (u_p) relation. It is assumed that the wave has reached a steady-state condition, which is reasonable, especially for the two higher pressure experiments, since the sample thicknesses are relatively thick (5 mm). However, experiments on thicker specimens would be necessary to confirm this hypothesis.

The strain rate $\dot{\epsilon}$ is determined from the measured plastic wave profiles. As mentioned earlier, the interface particle velocity histories are corrected to obtain the *in situ* particle velocity behind the shock front. These *in situ* particle velocity profiles are shown in Figure 5. The strain rate can be calculated using the relation,

$$\dot{\epsilon} = \frac{1}{U_s} \frac{du_p}{dt}, \tag{7}$$

where the time derivative is taken at the steepest part of the material velocity profile. The variation of shock stress and shock viscosity is shown plotted versus strain rate in Figure 6. A fourth-power dependence of the strain rate on the shock stress is also shown in the figure. The experiment at 2.9 GPa lies below the fourth-power curve indicated in the figure, possibly due to the shock wave not having reached steady state. Most materials require a significant propagation distance for the wave to evolve into a steady wave when shocked just above the Hugoniot elastic limit [3,17]. Also, at these low stresses, a different shock deformation mechanism may be responsible for the shock viscosity and hence would not necessarily give a fourth power dependence. A fit to the three data points indicated in the figure, however, would yield a third power dependence of the strain rate on the shock stress. Additional risetime experiments would be useful in establishing the exponent more accurately.

The composite risetime of the experimental system is approximately 3 ns. However, the perturbation caused by the epoxy bond sandwiched between the vanadium sample and the sapphire window is significant. It can be shown that a low-impedance material of shock impedance Z_g, when sandwiched between two similar high-impedance materials of shock impedance Z_m, acquires a particle velocity u_n in n reverberations, according to the relation,

$$\frac{u_n}{u_p} = \frac{2Z_m}{Z_g + Z_m} \frac{(1 - R^n)}{(1 - R)}, \tag{8}$$

where

$$R = (Z_g - Z_m)/(Z_g + Z_m), \tag{9}$$

and u_p is the peak particle velocity achieved. The shock impedance Z is defined as the product of the density of the material and its shock velocity. This is schematically depicted in the Lagrangian x-t diagram and the corresponding $\sigma - u$ diagram in Figure 7. The odd-numbered and even-numbered points represent states at the epoxy/mirror and sample/epoxy interfaces, respectively.

For the experiments reported in this paper, the number of reverberations required for the low-impedance epoxy adhesive to attain 90% of its peak value are 12, 10, and 8 respectively, at stress levels of 2.9 GPa, 6.4 GPa, and 9.7 Gpa. These correspond to reverberation times of 10, 7, and 5 ns respectively, for a bond thickness of 2.5 μm. These estimates are conservative, since for simplicity a constant shock impedance has been assumed for the epoxy bond to obtain the relation given by equation (8), and also since a shock impedance of sapphire has been assumed for vanadium. Nevertheless, the results indicate that for rapidly rising shock fronts, effects due to wave reverberations, such as an epoxy bond sandwiched between the sample and an interferometer window can be significant. This can be minimized by using extremely thin high impedance adhesives.

SHEAR STRESS IN THE SHOCKED STATE

The decrease in the interface particle velocity history indicated in Figure 2 represents the release states in the material. Stress relief in the vanadium sample is introduced by a low impedance backing to the sapphire impactor. The shock, generated in the sapphire disc upon impact reflects back as a release wave into the sapphire and sample. A knowledge of the equation of state for the sapphire combined with the known arrival time of the release wave at the sample-window interface is therefore sufficient to estimate the Lagrangian release wave speed in the material. The incremental relations given by equations (2) and (3) can be used to determine the stress relief paths for the material. The stress-strain release paths determined from the wave profiles are shown in Figure 8. Also shown in the figure are the present shock Hugoniot states and the isotherm for comparison. As indicated in the figure, the shock release states lie below the isotherm (which is assumed to be the hydrostat).

Shear stress estimates (normally defined as the yield strength) for the material, in the shocked state e_o, can be determined using the relation [18],

$$\tau_o + \tau_e = -(3/4)\rho_o \int_{e_o}^{e_p} (C_l^2 - C_b^2) de, \tag{10}$$

where ρ_o is the density of the material, C_l and C_b, are respectively the measured Lagrangian elastic release wave velocity and bulk velocity; e_p is the final strain state to which elastic-plastic effects are apparent. In this instance, C_b has been computed since the plastic portion of the wave is not well defined; this is especially true for experiments VA1 and VA2. The computed values for the bulk sound speed are based on Murnaghan's equation of state [16]. τ_o and τ_e, respectively, represent the shear stress state of the material in the shocked state and the equilibrium state after the shock passes through. These shear stress estimates determined using equation (10) are shown in Figure 9. As indicated in the figure, there is a decrease in shear stress with increasing shock stress beyond the Hugoniot elastic limit, suggesting shear softening in the shocked state. Normally, reshock experiments which exhibit elastic precursors [18] yield $\tau_e - \tau_o$, and are necessary to evaluate τ_e and τ_o, respectively. In the absence of such experiments, τ_o can be estimated from the stress deviator $(\sigma - P)$ at each stress level. These are shown plotted as $2\tau_o$ in Figure 9. As indicated in the figure, the estimates for $2\tau_o$ are comparable to $\tau_o + \tau_e$, suggesting that within the experimental uncertainty τ_o is equal to τ_e. Thus, reshock experiments if performed on vanadium over this stress range should not display an elastic precursor if heterogeneous and thermal trapping processes play a significant role at these stresses.

On the other hand, it is conceivable that the estimate of yield strength of 0.8 GPa is due to nonequilibrium rate effects due to dynamic loading, which asymptotes to its equilibrium value of ~0.43 GPa after passage of the shock wave. It should be noted that the static yield strength of the material is 0.44 GPa, which compares well with the estimates of the yield strength in the shocked state.

IV. SHOCK RECOVERY STUDIES

The shocked samples were recovered from the catcher tank which was filled with a very low impedance nylon material to cushion the impact assembly shown in Figure 1. The recovered samples were not flat discs, but were bowed due to edge relief effects. Since the impact surface was not marked, it is not clear as to whether the convex or concave surface is the impact interface.For metallographic analysis, discs from the

center of the specimens were used; metallographic analysis was also performed on an unshocked as-received specimen for comparison. Hardness measurements, optical microscopy and transmission electron microscopic techniques were used to investigate the microstructure induced in the shock-recovered specimens.

HARDNESS MEASUREMENTS

Rockwell A and Knoop microhardness measurements were used to characterize the residual properties of the shock-deformed vanadium. The Rockwell A hardness measurements were taken on both surfaces of the unshocked and shock-deformed plates. A minimum of five readings were taken for each measurement. The results of these measurements are reported in Figure 10. The results show that the hardness (in units of Rockwell A) increased from 21 to 33 for the concave surface and from 21 to 39 for the convex surface. Knoop microhardness readings, which utilized a 200-gram load and a 15-second holdtime, were taken through the thickness of the plate. These measurements have also suggested an increase in hardness in traversing from the concave side to the convex side. The variability in hardness measurements over the thickness of the specimen may have been due to the variable stress pulse duration in the sample from the impact interface to the sample/window interface.

OPTICAL METALLOGRAPHY

Optical micrographs of the unshocked and shock-deformed vanadium are shown in Figures 11(a) and 11(b). The grains in the unshocked material were equiaxed and ranged in size from 30 to 150 μm. An average grain size was not determined because of a bimodal grain size distribution. No evidence for inclusions or fine grain structure was observed. Optical microscopy showed that shock deformation had little or no effect on grain size. The grains, however, appeared to become more strained in the shock direction with increasing shock pressure. The primary change in optical microstructure caused by shock deformation was the development of fine deformation bands. These bands became more numerous with increasing shock pressure.

TRANSMISSION ELECTRON MICROSCOPY

Electron microscopy and diffraction were performed on a JEOL 200CX transmission electron microscope equipped with a goniometer stage at 200 kV. Thin-foil specimens for transmission electron microscopy (TEM) were prepared, both by electropolishing

and ion thinning. TEM of thin foils prepared by electropolishing, irrespective of the electrolyte used, revealed substructures containing numerous bands of platlets identified as ordered beta vanadium hydride. The presence of hydride in these samples was thought to be an artifact introduced during thinning. Similar hydride formation has been observed in vanadium foils thinned by chemical techniques [19-22]. The question of whether hydride was present in the vanadium was addressed by preparing thin foils by ion thinning. Ion-thinned samples were prepared using a Gatan Model 600 ion thinner at a gun voltage of approximately 6 keV and a beam current of 1 mA. The absence of hydride in ion-thinned foils showed conclusively that hydride was not present in either the unshocked or shock-deformed vanadium, but was an artifact of electropolishing.

TEM and electron diffraction from both electropolished and ion-thinned foils provided a more detailed description of the deformation structure than was obtained by optical metallography. Selected area-electron-diffraction studies indicated that the bands observed optically in the shock-deformed vanadium were deformation twins, which are shown in Figure 12. Diffraction analysis further showed that the twins belonged to the {112}<111> system, in agreement with that found previously for vanadium and other bcc metals [23]. Twinning occurred in all of the shock-deformed samples, but was not observed in the unshocked vanadium. The number of grains twinned and the twin density appeared to increase with increasing shock pressure, supporting the optical microscopy results. In grains of the 6.7-GPa and 9.7-GPa samples where twinning was observed, the twin spacing was typically 1 to 3 μm. No measure of the twin spacing in the 2.9-GPa sample was made and twin densities were not determined since the volume fraction of material examined in TEM could not be accurately determined. (It is conceivable that further analysis of the recovered specimens using SEM techniques may allow better estimates of twin-band spacing since a larger area will be sampled.) Normally, vanadium does not exhibit twin deformation patterns at room temperature under quasi-static loading, *i.e.*, at much lower strain rates than those reported in this study.

Another major shock deformation mode observed in vanadium was cross slip, which resulted in dense dislocation tangles. A typical array of tangled dislocations is also shown in Figure 12. Similar arrays were seen in all of the shock-deformed samples. The 10-GPa sample also contained a few grains which showed evidence for dislocation cell development. Dislocation densities measured for the unshocked and

shock-deformed vanadium suggest a rapid increase from an initial value of 7 x 10^8 cm^{-2} to 3 x 10^{10} cm^{-2} at 2.9 GPa; dislocation density measurements at the higher pressures suggest a saturated value of 9 x 10^{10} cm^{-2}. There was no evidence of either planar slip (*i.e.*, planar dislocation arrays) or shear banding in shock-deformed vanadium. Finally, no measurable difference in substructure was found after comparing thin foils taken from near the impact surface with those taken near the back surface.

V. DISCUSSION

Results of risetime measurements performed on vanadium, as expected, show steepening shock structure with increasing shock pressure. Although, the limited number of experiments reported in this study suggest a fourth-power dependence of the strain rate on the shock stress (as observed for other materials), further experiments would be useful in establishing the exponent more accurately. However, unlike aluminum [17] relatively large risetimes are observed, even at 9.7 GPa. This would imply that the deformation band spacing in vanadium should be greater than the micrometer spacing previously observed in aluminum [18], since a lower stress gradient over the shock front thickness would result in fewer deformation bands [24]. Although twin bands are observed in recovered specimens, it is not clear if they can be classified as shear deformation bands, since the twin bands are confined to a limited number of grains. In general, the deformation features observed suggest a lower dislocation density and a decreasing twin density with decreasing stress.

Both the shear-stress determinations and the shock-velocity measurements in vanadium suggest softening behavior, a phenomenon, which has been observed for high strength brittle materials such as quartz [9], sapphire [8], and tungsten [11]. (Vanadium, however, due to its high purity is very ductile, which was evidenced by the bowed shape of recovered specimens.) The reasons for material softening behavior are not understood; it is possible that strain-rate dependent processes allow a higher elastic shear stress (yield strength) to be sustained before relaxation to an equilibrium value of 0.43 GPa; it should be noted that this equilibrium value for the dynamic yield strength agrees well with the static yield strength of 0.44 GPa.

It is interesting to note that the dynamic behavior of vanadium is very similar to that of tungsten. Both materials have a body-centered cubic crystal structure, have relatively large Hugoniot elastic limits, and are high melting temperature metals. Both materials indicate a softening behavior but not a total collapse to the hydro-

stat; dislocation tangles and deformation twin bands are observed in shock-recovered specimens in either case.

The thermal diffusivity for vanadium is an order of magnitude lower than that for aluminum, and the deformation band spacing is expected to be much larger than that observed for aluminum at similar stresses; thermal recovery times would therefore be at least two orders of magnitude longer in vanadium than those calculated for aluminum, based on concepts of inhomogeneous deformation and thermal trapping [25-27]. In vanadium, since the thermal recovery times are comparatively long, an elastic precursor observed in other metals [18,28] in reshock experiments (due to thermal recovery from localized deformation processes) is not expected at these stresses. This is also evidenced by measurements of τ_o being comparable to τ_c. It is conceivable that material softening observed in vanadium is also a direct consequence of dissipative energy being deposited preferably in deformation twin bands which gives rise to a decrease in the yield (shear) strength for the material [26]. Since recovery times are long, the yield strength of the material does not recover during the time scales of these experiments. These concepts can be further pursued by performing experiments on thin specimens and by controlling the stress pulse duration in the specimen. In addition, reshock experiments on this material would be extremely useful to verify the concepts of thermal trapping and heterogeneous deformation, especially since the thermal diffusivity of vanadium is low compared to other metals.

VI. ACKNOWLEDGMENTS

We would like to acknowledge Dan Steinberg, Lawrence Livermore National Laboratory, for providing the samples used in this study.

VII. REFERENCES

1. R. A. Graham and J. R. Asay, *High Temp. - High Pressures,* 10, 355 (1978).

2. L. C. Chhabildas and J. R. Asay, *J. Appl. Phys.*, 50, 2749 (1979).

3. J. R. Asay, L. C. Chhabildas, and J. L. Wise, in *AIP Conference Proceedings* 78, 427 (1981).

4. D. E. Grady, "Spall Measurements in Uranium." this Conf. Proceedings.

5. J. W. Swegle and D. E. Grady, *J. Appl. Phys.* (in press).

6. D. E. Grady, W. J. Murri, and P. S. DeCarli, *J. Geophys. Res.* 80, 4857 (1975).

7. L. C. Chhabildas and D. E. Grady, in *Shock Waves in Condensed Matter*, J. R. Asay, R. A. Graham, and G. K. Straub eds., (Elsevier Science Publishers) 175 (1984).

8. R. A. Graham and W. P. Brooks, *J. Phys. Chem. Solids* 32, 2311 (1971).

9. R. A. Graham, *J. Phys. Chem. Solids* 35, 355 (1974).

10. D. P. Dandekar, *J. Appl. Phys.* 47, 4703 (1976).

11. J. R. Asay, L. C. Chhabildas, and D. P. Dandekar, *J. Appl. Phys.* 51, 4783 (1980).

12. L. M. Barker and R. E. Hollenbach, *Rev. Sci. Instrum.* 35, 742 (1964).

13. L. M. Barker and R. E. Hollenbach, *J. Appl. Phys.* 43, 4669 (1972).

14. L. M. Barker and R. E. Hollenbach, *J. Appl. Phys.* 41, 4208 (1970).

15. G. R. Gathers, A. C. Mitchell and N. C. Holmes, in *Shock Waves in Condensed Matter*, J. R. Asay, R. A. Graham, and G. K. Straub eds., (Elsevier Science Publishers) 89 (1983).

16. L. C. Ming and M. H. Manghnani, in *High-Pressure Science and Technology*, K. D. Timmerhaus and M. S. Barber, eds., (Plenum Publishing Corporation), V1, 54 (1979).

17. J. N. Johnson and L. M. Barker, *J. Appl. Phys.* 40, 4321, (1969).

18. J. R. Asay and L. C. Chhabildas, in *Shock Waves and High-Strain-Rate Phenomena in Metals*, ed. by M. A. Meyers and L. E. Murr, Plenum Publ. (1981).

19. Shigeo Takano and Taira Suzuki, *Acta Metallurgica* 22, 265 (1974).

20. M. P. Cassidy, B. C. Muddle, T. E. Scott, C. M. Wayman, *Acta Metallurgica* 25, 829-838 (1977).

21. R. Bolsing, E. Braun, U. Hauber, and M. Ruhle, *Praktische Metallog.* 6, 475 (1969).

22. P. B. Hirsch, A. Howie, R. B. Nicholson, D. W. Pashley, and M. J. Whelan, *Electron Microscopy of Thin Crystals*, Butterworth, Inc., Washington, DC, 422 (1965).

23. T. C. Lindley and R. E. Smallman, *Acta Metallurgica* 11, 361-371 (1963).

24. D. B. Hayes and D. E. Grady, in *AIP Conference Proceedings*, 78, 412 (1981).

25. D. E. Grady and J. R. Asay, *J. Appl. Phys.* 53, 7350 (1982).

26. J. W. Swegle and D. E. Grady, "Calculation of Thermal Trapping in Shear Bands," this Conference Proceedings.

27. Lee Davison and R. A. Graham, in *Physics Reports* 55, 302 (1979).

28. L. C. Chhabildas, J. L. Wise, and J. R. Asay, in *AIP Conference Proceedings*, 78, 422 (1981).

Figure Captions

FIG. 1. Experimental impact configuration to determine shock loading and release states in vanadium.

FIG. 2. Interface particle velocity histories measured at the sample-window interface.

FIG. 3. Comparison of present shock velocity-particle velocity measurements with results previously reported in reference 15.

FIG. 4. Comparison of present Hugoniot states with the hydrostat and a Hugoniot based on an elastic-perfectly-plastic model. Present data suggest material softening.

FIG. 5. Particle velocity loading histories in vanadium obtained from the interface particle velocity histories shown in FIG. 2.

FIG. 6. Variation of shock stress and effective shock viscosity with strain-rate. The solid line represnts a fourth power dependence of the strain rate on the shock stress while the small-dashed line represents a third power dependence.

FIG. 7. Lagrangian x-t and σ-u diagram, indicating the reverberation of an epoxy bond sandwiched between the sample and window.

FIG. 8. Stress-strain diagram depicting the loading and release paths determined from particle velocity histories in FIG. 4.

FIG. 9. Shear stress (yield strength) estimates obtained using equation (10) and from stress deviator estimates indicated in Figures (4) or (8).

FIG. 10. Rockwell A hardness measurements, indicating an increase in hardness with increasing shock stress. Note also the difference in hardness measurements for the two surfaces.

FIG. 11. Optical micrographs of the (a) unshocked and (b) 9.7-GPa shock deformed vanadium.

FIG. 12. TEM micrographs of the 6.7-GPa shocked specimen, indicating twins superposed on a network of dislocation tangles.

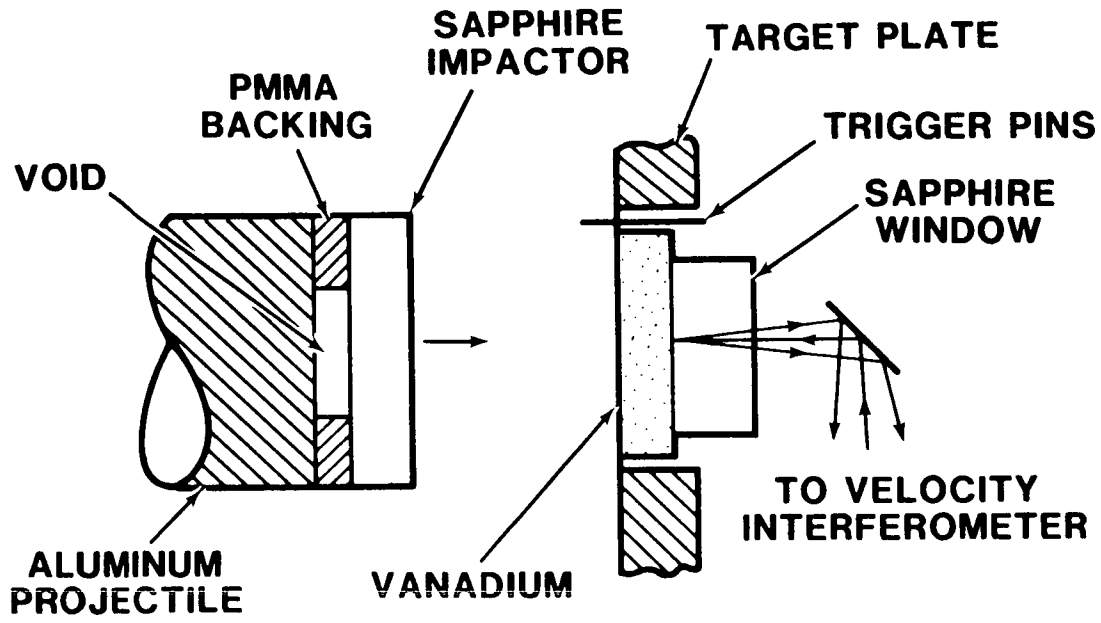
SAPPHIRE
IMPACTOR
TARGET PLATE
PMMA
BACKING
TRIGGER PINS
VOID
SAPPHIRE
WINDOW
TO VELOCITY
INTERFEROMETER
ALUMINUM
PROJECTILE
VANADIUM

Figure 1

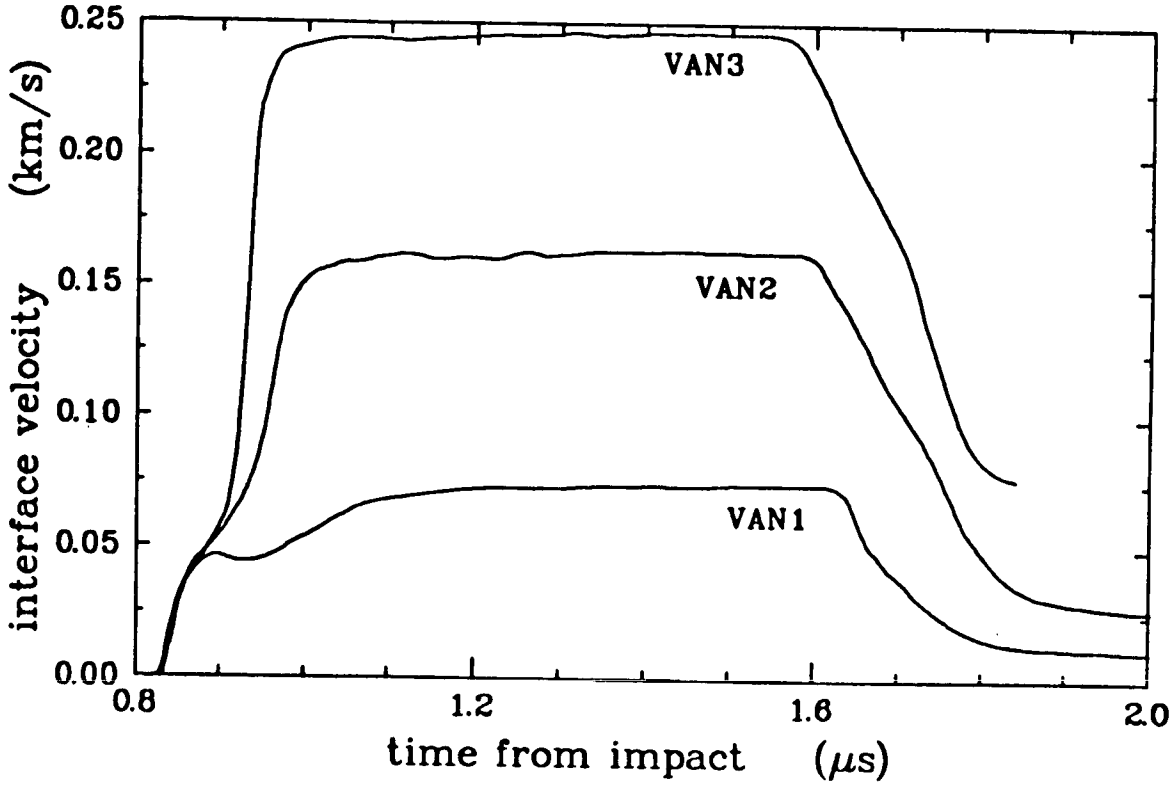
0.25
0.20
0.15
0.10
0.05
0.00
interface velocity (km/s)
VAN3
VAN2
VAN1
0.8
1.2
1.6
2.0
time from impact (μs)

Figure 2

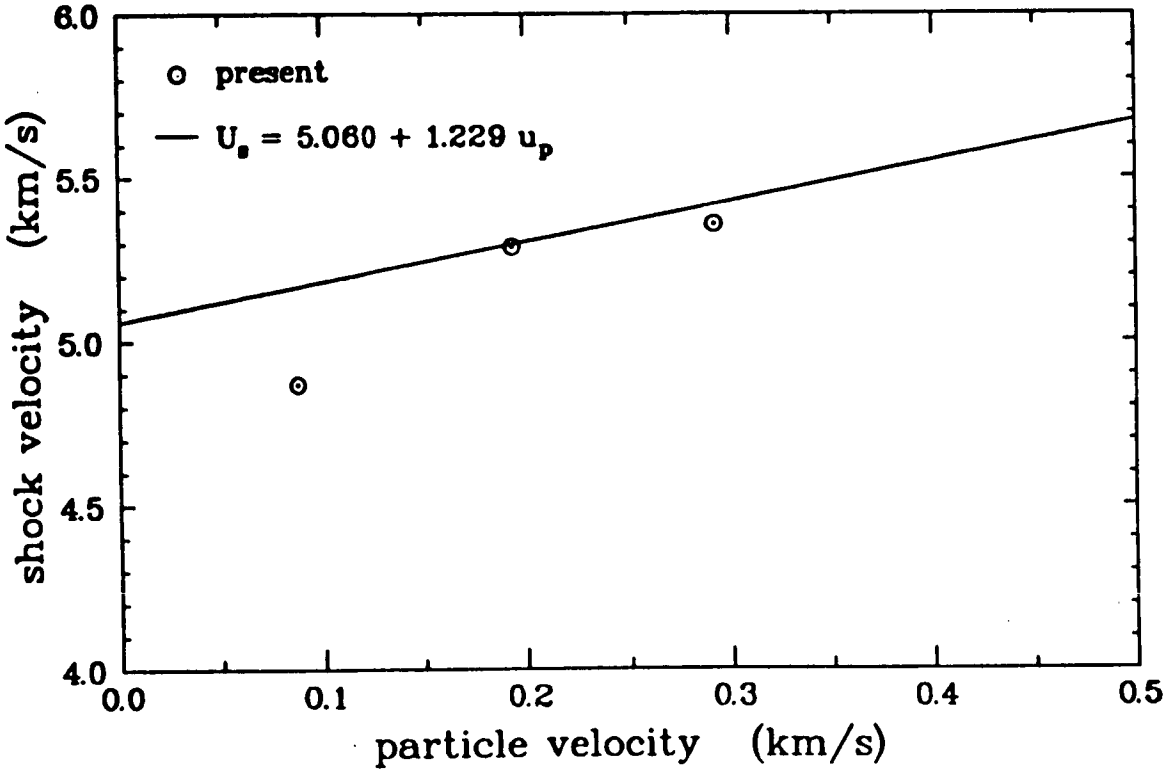
6.0
5.5
5.0
4.5
4.0
shock velocity (km/s)
o present
— $U_s = 5.060 + 1.229\ u_p$
0.0
0.1
0.2
0.3
0.4
0.5
particle velocity (km/s)

Figure 3

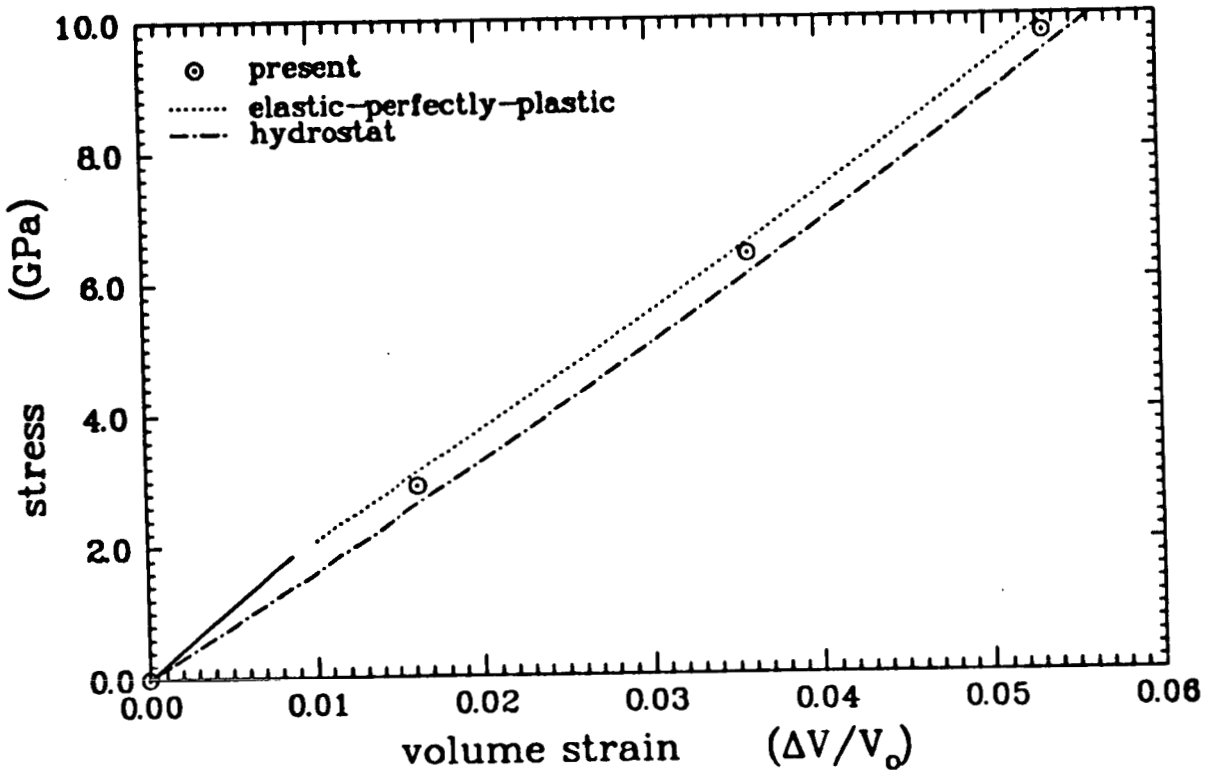
present
elastic–perfectly–plastic
hydrostat
10.0
8.0
6.0
4.0
2.0
0.0
stress (GPa)
0.00
0.01
0.02
0.03
0.04
0.05
0.06
volume strain (ΔV/V$_o$)

Figure 4

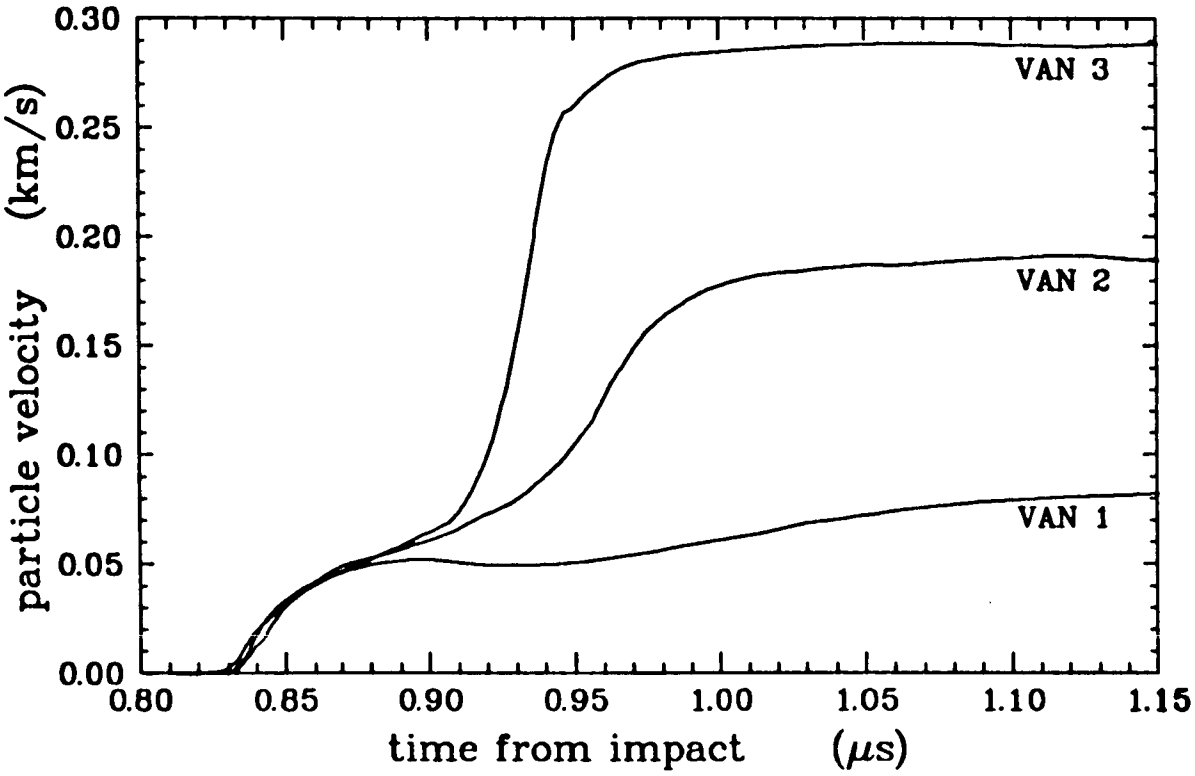
0.30
0.25
0.20
0.15
0.10
0.05
0.00
particle velocity (km/s)
VAN 3
VAN 2
VAN 1
0.80
0.85
0.90
0.95
1.00
1.05
1.10
1.15
time from impact (μs)

Figure 5

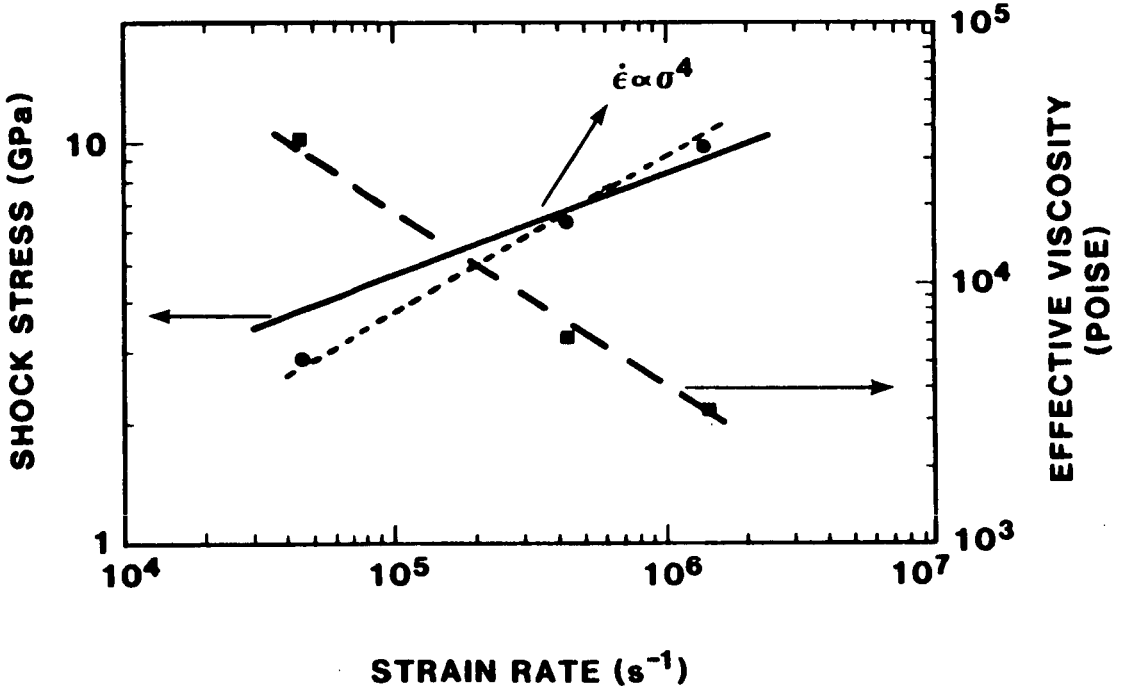
SHOCK STRESS (GPa)
10
1
10^4
10^5
10^6
10^7
STRAIN RATE (s^{-1})
$\dot{\epsilon} \propto \sigma^4$
10^5
10^4
10^3
EFFECTIVE VISCOSITY (POISE)

Figure 6

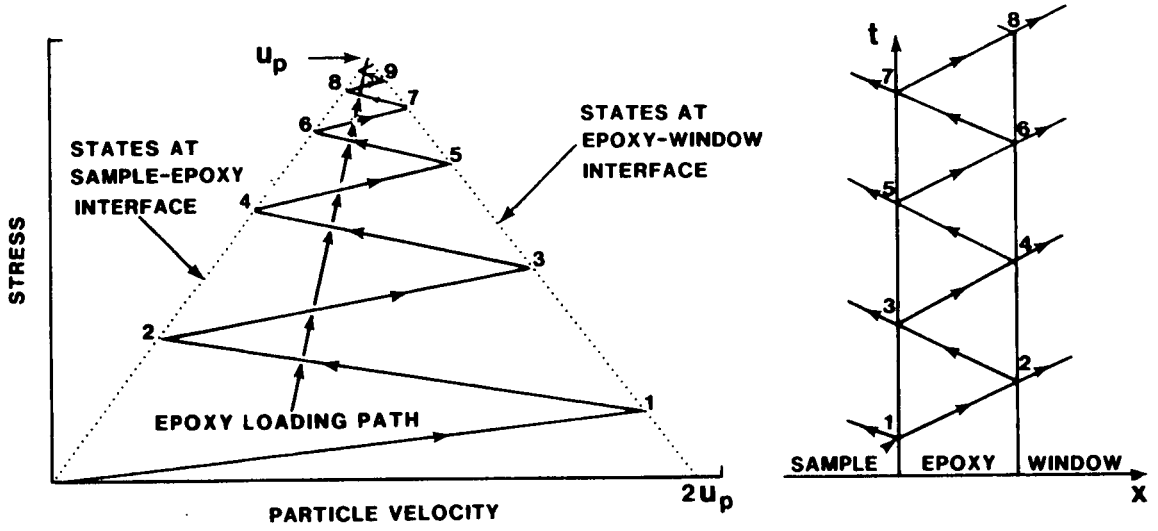
u_p
STATES AT
SAMPLE-EPOXY
INTERFACE
STATES AT
EPOXY-WINDOW
INTERFACE
STRESS
EPOXY LOADING PATH
PARTICLE VELOCITY
$2u_p$
t
SAMPLE
EPOXY
WINDOW
X

Figure 7

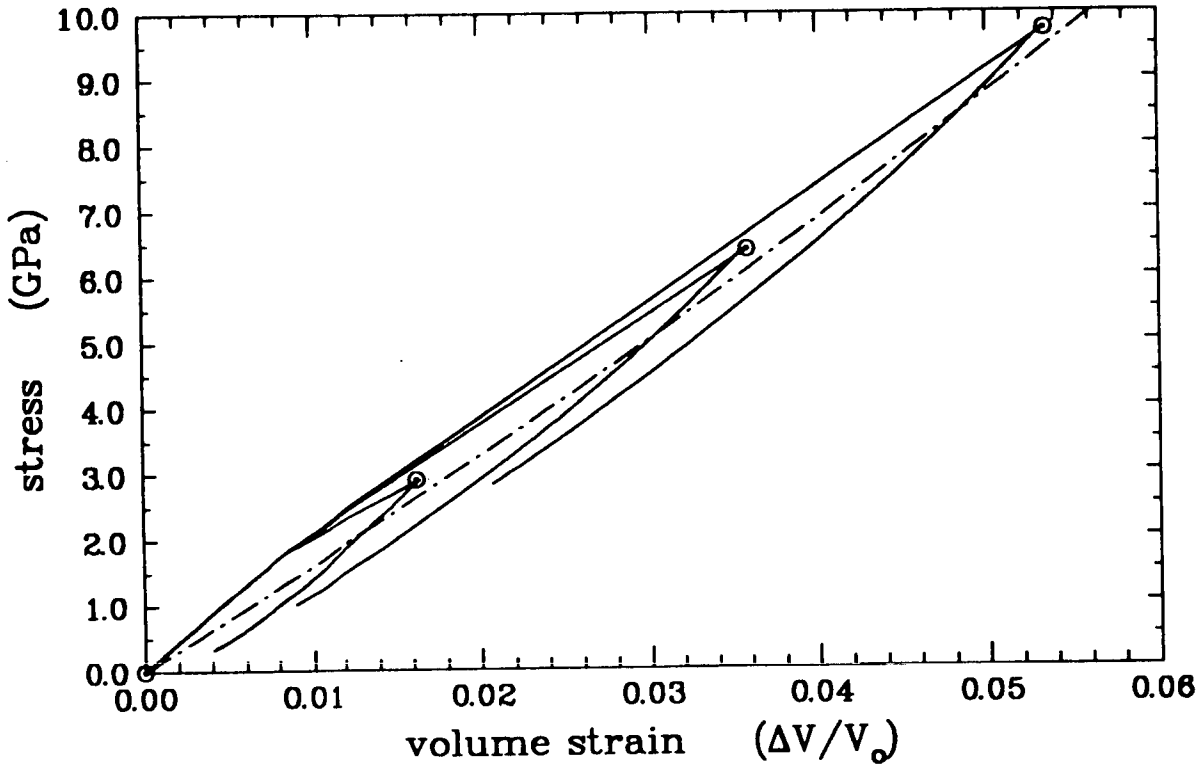
10.0
9.0
8.0
7.0
6.0
5.0
4.0
3.0
2.0
1.0
0.0
stress (GPa)
0.00
0.01
0.02
0.03
0.04
0.05
0.06
volume strain (ΔV/V$_o$)

Figure 8

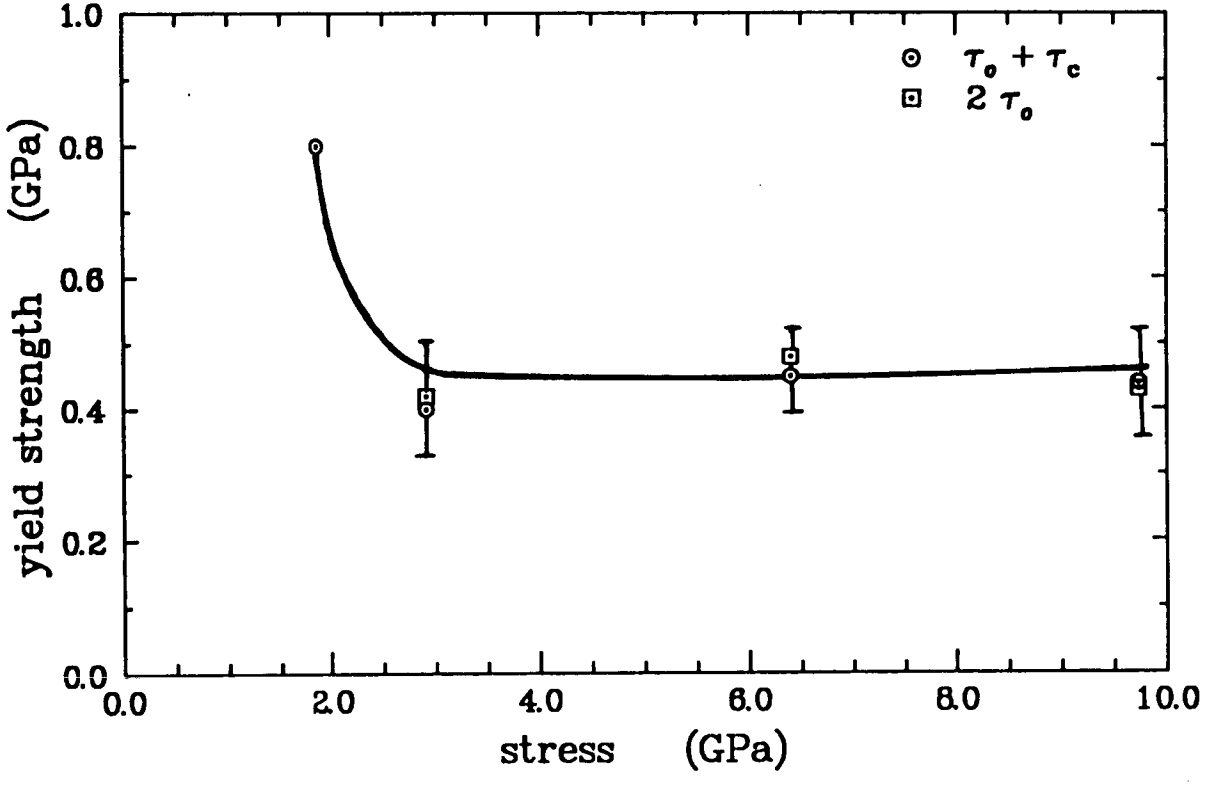
1.0
0.8
0.6
0.4
0.2
0.0
yield strength (GPa)
0.0
2.0
4.0
6.0
8.0
10.0
stress (GPa)
$\tau_0 + \tau_c$
$2\tau_0$

Figure 9

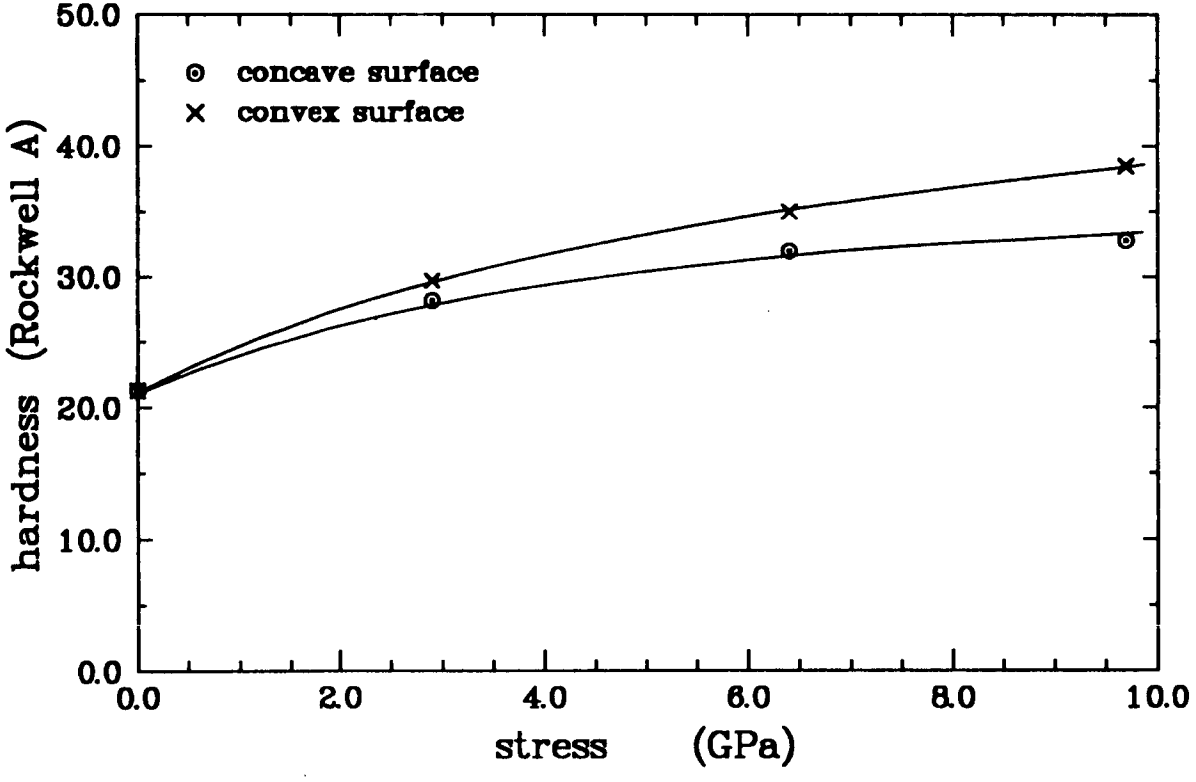
50.0
40.0
30.0
20.0
10.0
0.0
hardness (Rockwell A)
concave surface
convex surface
0.0
2.0
4.0
6.0
8.0
10.0
stress (GPa)

Figure 10

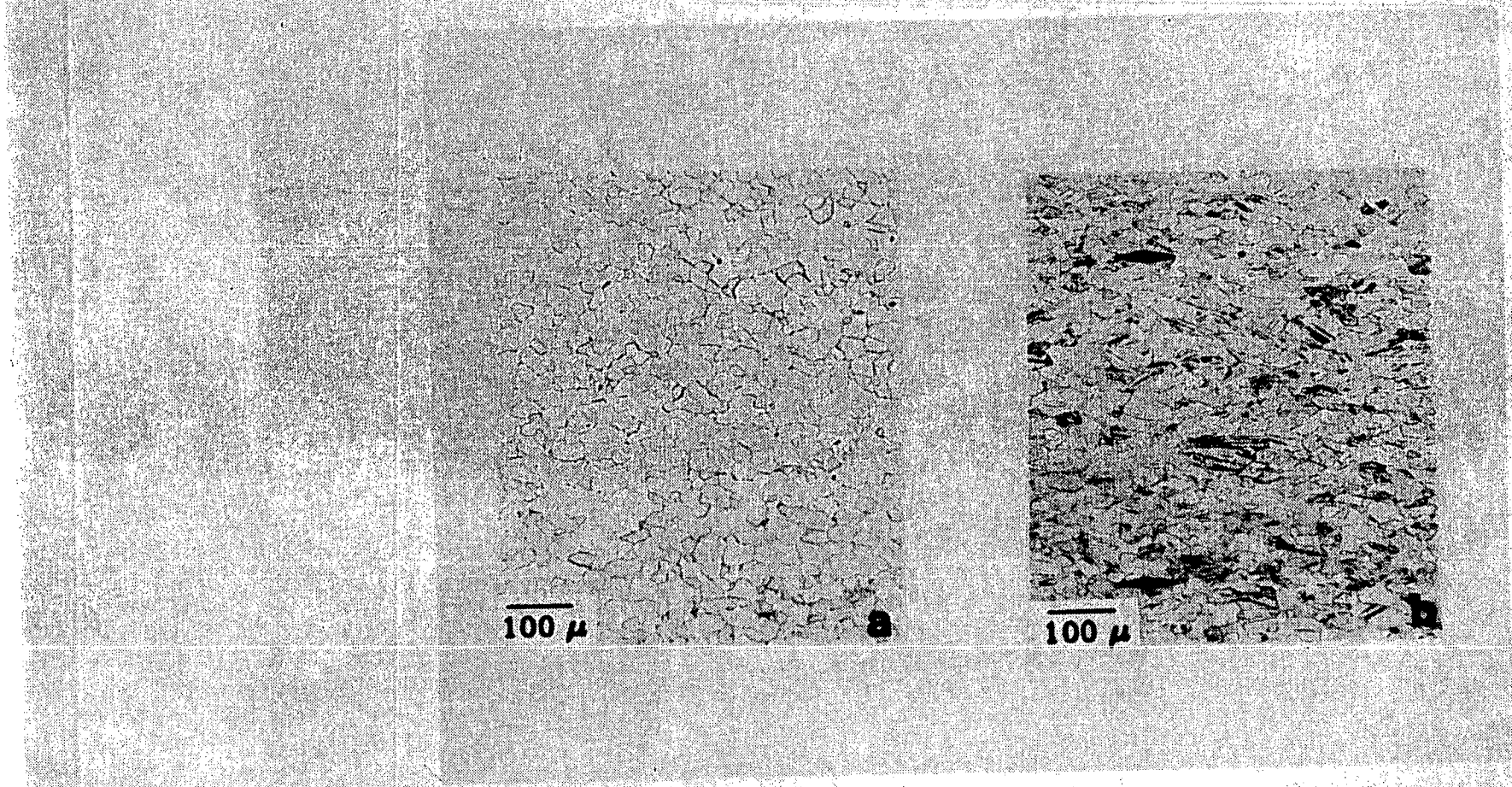

Figure 11

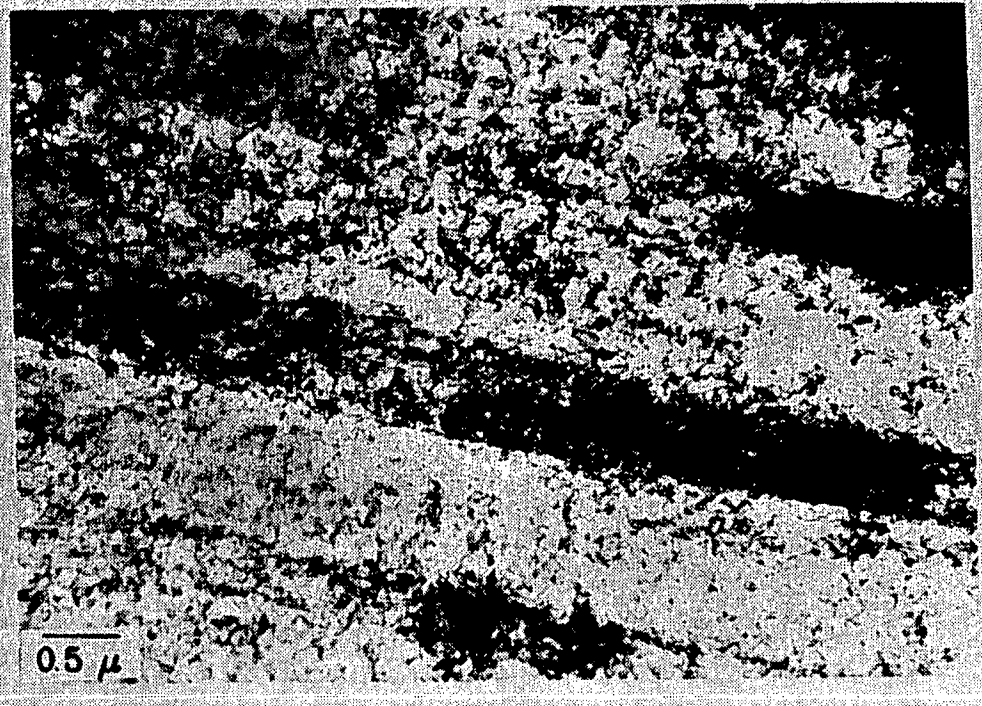

Figure 12